

## Modelling an Acoustically Perturbed Rocket Engine Combustion Chamber with Cryogenic Propellant Injection

S.K. Beinke<sup>1,2</sup>, D.T. Banuti<sup>3</sup>, J.S. Hardi<sup>2</sup>, M. Oswald<sup>2</sup>, and B.B. Dally<sup>1</sup>

<sup>1</sup> School of Mechanical Engineering  
The University of Adelaide  
Adelaide 5005, South Australia, Australia

<sup>2</sup>Institute of Space Propulsion  
German Aerospace Center (DLR)  
Lampoldshausen, D-74239 Hardthausen, Germany

<sup>3</sup>Institute for Aerodynamics and Flow Technology  
German Aerospace Center (DLR)  
Göttingen, 37073 Göttingen, Germany

### Abstract

An experimental combustor, dubbed BKH, has been developed at DLR Lampoldshausen to investigate combustion instability phenomena. The combustor operates with cryogenic liquid oxygen and hydrogen propellants at supercritical pressure conditions analogous to real rocket engines. The BKH combustor has been modelled using a specially developed version of the DLR TAU code with real gas capabilities for supercritical injection. The TAU code CFD results are compared with optical data recorded during BKH experiments. The numerical flame and liquid oxygen distributions match experimental observations. The acoustic field inside the BKH combustor has also been calculated separately with an acoustic solver that uses a realistic acoustic property distribution from the CFD calculations. The resonant modes are successfully predicted using the acoustic solver.

### Introduction

Combustion instabilities refer to a spontaneously developing and self-sustaining coupling between acoustic and combustion processes inside combustion chambers. Acoustic pressure disturbances may interact with combustion processes such that mutual reinforcement occurs. If left unchecked, the amplitude of the pressure fluctuations may grow and affect the internal flow field within the combustion chamber. If the instability is large enough it can compromise the structure or affect the operation and lifetime of the combustion chamber, possibly leading to a premature failure of the engine and loss of a rocket mission.

High frequency combustion instabilities, occurring at frequencies greater than 1000 Hz, are the least understood and most damaging type of instability. At high frequencies the acoustic behaviour is attributed to the resonant modes of the combustion chamber volume. To ensure an engine is free from combustion instabilities before operation extensive ground testing is conducted over the engine's operational envelope. Ground testing adds significant time and cost to the development of new rocket engines. The ability to accurately predict combustion instabilities during the design phase with numerical tools would reduce risk and allow for more economical rocket engine development. However, before such tools can be applied they must be developed and validated against experimental results.

The goal of the current work is to develop a method to model an experimental combustion chamber (dubbed BKH) that is used to conduct combustion instability research at the DLR institute of space propulsion. The developed modelling methodology will be used to gain further insight into the BKH experiments and to conduct additional numerical investigations to study combustion instability phenomena. This paper presents the initial work to model the internal combustor flow field and the excited acoustic fields inside the BKH combustion chamber. The numerical results are compared against available experimental data.

### Experimental Setup

The BKH combustor operates at pressures ranging from 40 bar (sub-critical oxygen pressure) to 60 bar (super-critical oxygen pressure) using cryogenic liquid oxygen (LOx) and hydrogen (H<sub>2</sub>) propellants. The combustion chamber features a rectangular geometry with windows located on each side for optical access to the near injector region, and a secondary nozzle and siren wheel for excitation. The combustion chamber volume is 240 mm long, 50 mm wide and 200 mm high, not including the main and secondary nozzles. Figure 1 depicts the BKH chamber configuration.

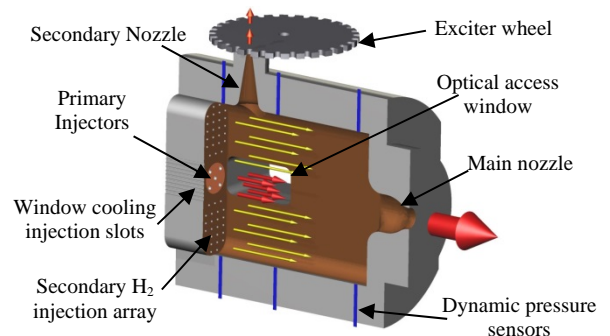


Figure 1. Concept diagram of the BKH combustion Chamber

During operation the exciter wheel is rotated at a controlled speed in order to periodically interrupt the flow through the secondary nozzle. This causes an acoustic disturbance to propagate back into the chamber. Dynamic pressure measurements are recorded at various locations on the combustion chamber wall to resolve the acoustic field.

The response of the study elements to the acoustic disturbance is observed via high speed shadowgraph and OH chemiluminescence (OH\*) imaging captured through the optical windows. The rectangular shaped internal volume was designed to limit the orientations of transverse acoustic modes and match the resonant mode frequencies of full-scale upper-stage rocket engines. BKH experiments are conducted at the European Research and Technology test Facility P8 for cryogenic rocket engines at DLR Lampoldshausen. Additional information on BKH can be found in references [4–6].

The current work aims to model the reacting flow, at 60 bar within the chamber with a ratio of oxidiser to fuel (ROF) of 6. As the chamber pressure is above the supercritical pressure of all of the injected species, liquid and gaseous phases do no longer exist and thus need not be distinguished in the model. The experimental data presented is from an experiment where the excitation system was not in operation. Random combustion noise from the study elements weakly excites the resonant modes of the combustion chamber.

### Flow Field Modelling

CFD calculations of the internal BKH flow field were computed using a specialised version of the DLR TAU code which accounts for real gas properties. In this section the DLR TAU code and the applied modelling parameters are described.

The DLR TAU code is a hybrid (structured/unstructured) grid Godunov-type finite-volume flow solver for the compressible Euler and Navier-Stokes equations. Spatial second order is reached by a MUSCL reconstruction. The TAU code has been validated for a range of steady and unsteady flow cases [3,7].

For the current work, the one-equation Spalart-Allmaras [10] turbulence model was used for simplicity. A MAPS+ Riemann solver is used to handle low Mach numbers and high density gradients. Stabilization, if necessary for the computation of high density ratio shear layers, is carried out by reducing the spatial order to 1.95. In this way, the numerical damping is minimally increased while mass, momentum, and energy remain conserved. A finite rate chemistry scheme that solves the Arrhenius equation is used in the current work. The Jachimowski mechanism is described by [9] and involves 8 species and 17 reactions.

Cryogenic oxygen at high pressures, as encountered in rocket engines, behaves differently than ideal gases. To account for these real gas effects, a new real gas mixture model has been developed and implemented in the DLR TAU code. The model, and its validation, are described in more depth in [1,2].

In this new model, cryogenic oxygen is treated as an Eulerian continuum. Real gas properties are computed from the high fidelity modified Benedict-Webb-Rubin (MBWR) equation of state (EOS) of Younglove [11] and stored in a library during a pre-processing step. Thermodynamic state variables, such as pressure, enthalpy, heat capacities, speed of sound, etc. are all computed consistently from the real gas EOS. Real gas corrections to the transport coefficients are evaluated following Lemmon and Jacobsen [8]. Here, an ideal gas equation is solved for each of the species  $H_2$ ,  $OH$ ,  $H_2O$ ,  $H_2O_2$ ,  $O$ ,  $H$ ,  $HO_2$ , and the real gas MBWR library is used for  $O_2$ .

The domain used for the CFD calculations is shown in Figure 2. Vertical symmetry was used to reduce the size of the numerical domain. It includes 10 mm of each of the injection elements leading up to the injection plane. It also includes extensions at the main and secondary nozzles to ensure that the sonic flow through each of the nozzles, which do not have smooth expansion sections, is captured.

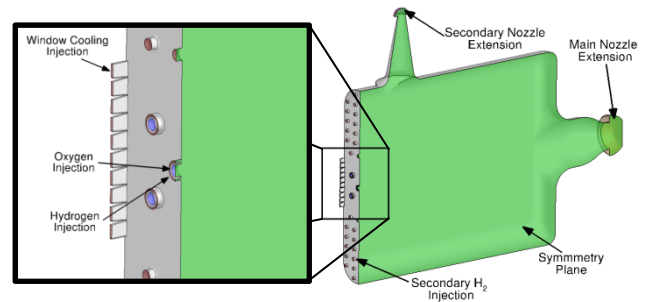


Figure 2. Numerical domain and boundary conditions used for CFD calculations.

A hybrid structured/unstructured mesh consisting of approximately 1.7 million nodes was generated for the domain. The mesh applied a structured prismatic boundary layer along the walls and an unstructured tetrahedral mesh to fill the internal volume. The mesh was refined near the LOx post tips and in the flame zone. A symmetry boundary condition was applied to the vertical symmetry plane of the chamber. Exit pressure outflow boundaries at atmospheric conditions were used at the main and secondary nozzle boundary surfaces. Dirichlet boundary conditions were prescribed for each of the injectors based on an assumed pressure drop across the feed system. Thus the mass flow and state of the fluid entering the domain is set absolutely.

All of the walls of the chamber were treated as non-slip boundaries. The BKH chamber is actively cooled during operation and the chamber wall temperature does not change significantly during steady operation. To permit thermal losses through the walls of the chamber an isothermal temperature distribution was prescribed. This temperature distribution was estimated based on wall temperature measurements recorded from BKH experiments at similar operating points.

### Acoustic Field Modelling

The goal of modelling the acoustic field is to identify the resonant mode frequencies and distributions within the BKH combustion chamber. CFD simulations of the chamber under excitation are computationally expensive. A more economical approach using a separate acoustic solver, COMSOL Multiphysics, is employed.

COMSOL Multiphysics is a commercial tool with various modules for modelling different physical problems. For the current work the pressure acoustics model which is part of the acoustics module was used for the current work. The pressure acoustics solver solves the wave equation for a perfect gas. One advantage of COMSOL Multiphysics is the capability to import property distributions. This allowed a mean flow field property distribution calculated using the DLR TAU code to be imported. The acoustic wave equation was then solved with consideration of the acoustic property distribution within the combustion chamber volume. The wave equation in the frequency domain is

$$\nabla \cdot \left( -\frac{1}{\rho_c} \nabla p \right) + \frac{\lambda^2 p}{\rho_c c_c^2} = 0 \quad (1)$$

where  $p$  is the acoustic pressure,  $\lambda$  is the eigenvalue,  $\rho_c$  and  $c_c$  are the mean flow density and speed of sound, respectively.

The domain used for the modal analysis was similar to that used for the CFD calculations. Vertical symmetry was used to reduce the domain to one half of the BKH chamber. The injection elements themselves were ignored and the injection plane was instead treated as a uniform flat wall. The main and secondary nozzle geometries were cut off at the throat and replaced with a solid wall boundary condition.

The domain was meshed using approx. 300,000 tetrahedral elements as shown in Figure 3 (left). An interpolation function was prescribed to map the results from a steady state RANS simulation of the BKH combustor to each point in the mesh. The mapped variables came from an ideal gas calculation of the BKH combustor the same 60 bar ROF 6 operating point as the real gas CFD calculations. The ideal gas calculation is only different in that all species are treated as an ideal gas, including oxygen. This simplification was considered an acceptable compromise as it provides better results than the application of a single-valued, homogeneous property distribution. The speed of sound distribution taken from the ideal gas calculation and applied for the modal analysis is shown in Figure 3 (right). The MUMPS eigenvalue solver was applied to calculate the eigen frequencies and mode shapes using COMSOL.

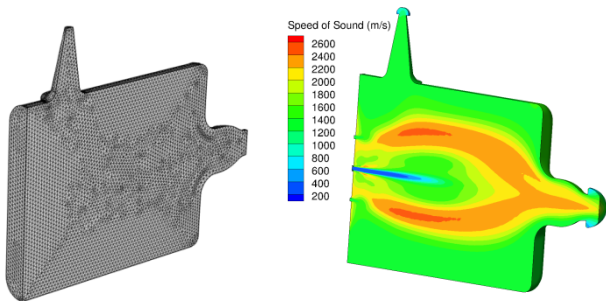


Figure 3. Domain and mesh used for modal analysis (Left) and speed of sound distribution calculated using ideal gas assumption with TAU as applied for modal analysis (Right).

**Results and Discussion**

In this section the relevant experimental and numerical results are compared. Visualisations of the CFD results of the internal flow field are compared with available experimental optical data. The identified acoustic fields from the modal analysis are compared with dynamic pressure data from a BKH experiment.

**Flow Field Results**

High speed OH\* and shadowgraph images have been collected during a BKH experiment. The images are recorded via line of sight access from the side of the chamber as shown in Figure 4. Due to the penta-injector configuration, two of the five injection elements are hidden behind other elements and only 3 distinct jets are visible in the images.

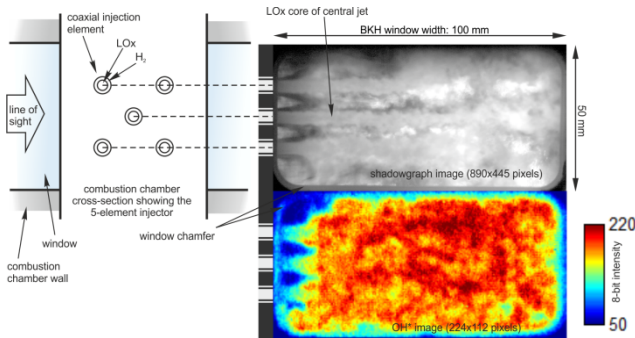


Figure 4. Optical line of sight shadowgraph (top) and OH\* (bottom) instantaneous imaging results from BKH experiments.

The resulting high speed videos were time averaged to produce mean images for comparison with the RANS CFD results. Figure 5 shows a comparison of the density distribution from the CFD results and a time averaged sample of shadowgraph data. Injection is from the left to the right side of the image. Lines following the centre of the dense liquid oxygen jets from the TAU results have been drawn over both images.

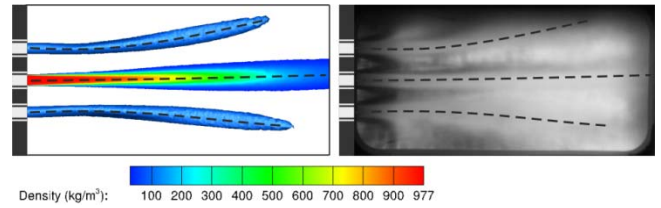


Figure 5. Post processed TAU result showing the density distribution in the window region (Left) and time averaged shadowgraph image recorded during BKH experiment (Right). The displayed density in the TAU results is cut off and iso surfaces are shown at a value of 100 kg/m³.

The images in Figure 5 show good agreement. The central jet is observed to extend the length of the window region in both cases, and the upper and lower jets are deflected away from the central jet. The upper jet is deflected slightly more than the lower jet due to the influence of the secondary nozzle. The LOx jets in the numerical solution appear to be longer and deflect later than the experimental results. Only a qualitative comparison of the results is possible as the exact density gradients observed in the experiment data are unknown.

Figure 6 shows a comparison of the observed OH\* distribution in the window region and the OH mass fraction distribution in the CFD results. The same lines following the centre of the dense oxygen jets as shown in Figure 5 are overlaid on the image. Additional lines showing the edge of the OH mass fraction distribution from the numerical results are also shown. In the experiment the flame fills almost the entirety of the window region while the CFD results show individual jets propagating further into the chamber before mixing together into a uniform OH distribution.

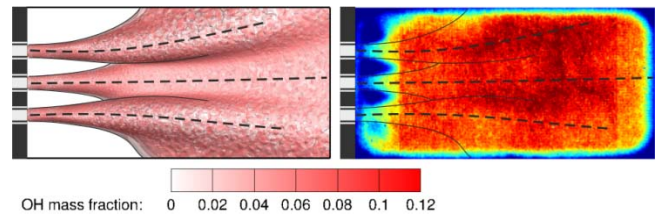


Figure 6. OH image comparison. Post-processed TAU code result showing iso surfaces at OH mass fraction = 0.04, 0.08, & 0.12 (Left) and time averaged OH\* image recorded during BKH experiment (Right).

Both types of optical data suggest that the numerical results exhibit longer, more intact jets than the experiment. The assumed pressure drop across the feed system may be incorrect leading the species injected numerically to have a higher enthalpy and momentum than the experiment. This will be investigated in future work.

**Acoustic Field Results**

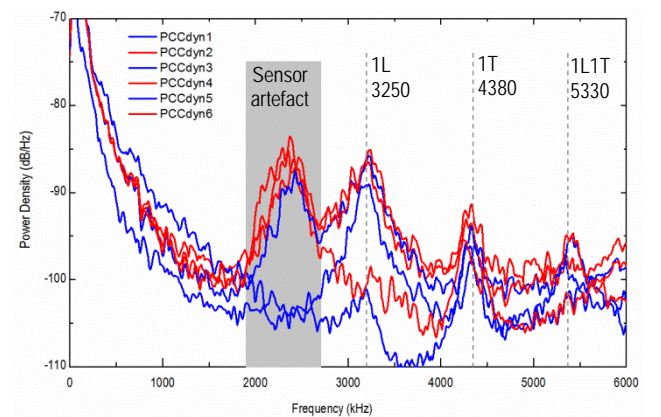


Figure 7. PSD of dynamic pressure data during BKH experiment without excitation.

The acoustic field is observed experimentally using wall mounted dynamic pressure sensors with a sampling rate of 100 kHz. Figure 7 shows the spectrum of the recorded dynamic pressure data. The first peak in Figure 7 at approximately 2500 Hz has been identified as a sensor artefact. The following peaks at 3250 Hz and 4350 Hz are the 1L and 1T modes, respectively.

An eigenmode calculation was computed using COMSOL Multiphysics as described earlier. The computed eigen-modes and eigen-frequencies are listed in Table 1. In reality, as shown in Figure 7, the resonant modes peaks are quite broad and it is difficult to identify a single resonant frequency. The calculated mode frequencies correspond well with those observed experimentally.

Eigen-mode	Eigen-frequency (Hz)		Error (%)
	Experiment	COMSOL	
1L	3250	3288	1.2
1T	4350	4381	0.7

Table 1 Identified eigen-modes and eigen-frequencies

Figure 8 shows the calculated 1L and 1T mode pressure distributions at the centre plane of the chamber. The influence of the mean flow field can be seen most clearly in the 1T mode result. The pressure distribution is distorted in the axial direction, from the injection plane to the main nozzle, where hot combustion products circulate leading to a higher speed of sound. Without the mean flow property distribution, the pressure contours would remain horizontal along the length of the chamber.

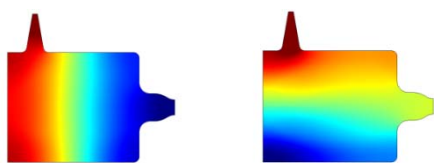


Figure 8. Calculated 1L (Left) and 1T (Right) mode pressure distributions

The pressure distributions qualitatively match those expected for each of the acoustic modes. Additional work will be done to study the effect of the boundary conditions at the main and secondary nozzles, and the influence of the feed system. It is expected that by using more realistic boundary conditions, and a speed of sound distribution extracted from the real gas calculation, better agreement with experimental values can be obtained.

## Conclusion

A steady state simulation of the BKH combustion chamber has been computed using a specialised version of the DLR TAU code designed to model combustion of species with real gas properties. The results have been post-processed and compared with available optical data from BKH experiments. The numerical results exhibit similar flame and LOx jet distributions as observed experimentally. These results are expected to improve markedly with further consideration of the injection boundary conditions.

A methodology for performing a modal analysis with consideration of the acoustic property distribution has been demonstrated. The numerical results agree well with the experiment. More sophisticated acoustic property distributions, boundary conditions, and models that may improve upon the current results will be investigated in the future.

In the future the identified frequencies and distributions from the modal analysis will be used to generate boundary conditions for acoustic excitation. The boundary conditions will be imposed onto unsteady CFD simulations of BKH study elements to study the elements response to the acoustic disturbance.

## Acknowledgments

This work is conducted within the scope of the DLR Pro-Tau project. The authors would like to thank Bernd Wagner, Sebastian Karl, Volker Hannemann, and the members of the Aerodynamics and Flow Technology group at DLR Göttingen for the continued support and expertise provided. The authors would also like to thank Samuel Webster and Jeremy Chan from DLR Lampoldshausen for helpful conversations and assistance provided.

Research undertaken for this report has been assisted with a grant from the Sir Ross and Sir Keith Smith Fund (Smith Fund) ([www.smithfund.org.au](http://www.smithfund.org.au)). The support is acknowledged and greatly appreciated. The Smith Fund by providing funding for this project does not verify the accuracy of any findings or any representations contained in it. Any reliance on the findings in any written report or information provided to you should be based solely on your own assessment and conclusions. The Smith fund does not accept any responsibility or liability from any person, company or entity that may have relied on any written report or representations contained in this report if that person, company or entity suffers any loss (financial or otherwise) as a result.

## References

- [1] Banuti, D. & Hannemann, K., Efficient multiphase rocket propellant injection model with high quality equation of state, *4th Space Propulsion Conference*, 2014.
- [2] Banuti, D.T. & Hannemann, K., Real gas library in continous phase propellant injection model for liquid rocket engines, in *49th AIAA Joint Propulsion Conference*, San Jose, 2013.
- [3] Gerhold, T., Hannemann, V., & Schwamborn, D., On the Validation of the DLR-TAU Code, *New Results in Numerical and Experimental Fluid Mechanics, Notes on Numerical Fluid Mechanics*, editors R.H. W. Nitsche and H.-J. Heinemann, 1999: pp. 426–433.
- [4] Hardi, J., Gomez Martinez, H.C., Oswald, M., & Dally, B., LOx jet atomization under transverse acoustic oscillations, *Journal of Propulsion and Power* **30**, 2014, 337–349.
- [5] Hardi, J., Oswald, M. & Dally, B., Flame response to acoustic excitation in a rectangular rocket combustor with LOx/H2 propellants, *CEAS Space Journal*, **2**, 2011, 41–49.
- [6] Hardi, J.S., *Experimental Investigation of High Frequency Combustion Instability in Cryogenic Oxygen-Hydrogen Rocket Engines*, The University of Adelaide, 2012.
- [7] Karl, S., *Numerical Investigation of a Generic Scramjet Configuration*, Technische Universität Dresden, 2011.
- [8] Lemmon, E.W. & Jacobsen, R.T., Viscosity and thermal conductivity equations for nitrogen, oxygen, argon, and air., *International Journal of Thermophysics* **25(1)** 2004, 21–69.
- [9] Lempke, M. Gerlinger, P. & Aigner, M., Assumed PDF Modeling in Rocket Combustor Simulations, *4th European Conference on Aerospace Sciences*, 2011.
- [10] Spalart, P.R. & Allmaras, S.R., A One-Equation Turbulence Model for Aerodynamic Flows, *AIAA paper*. 1992.
- [11] Younglove, B.A., Thermophysical Properties of fluids. 1. Argon, ethylene, parahydrogen, nitrogen, nitrogen trifluoride and oxygen, *Journal of Physical and Chemical Reference Data*. **11** 1982 Supplement No. 1.